Novel continuum models for coupled shear wall analysis

Antonio Capsoni[1] and Hadi Moghadasi Faridani[2*,†]

[1]*Department of Architecture, Built Environment and Construction Engineering, Politecnico di Milano, Milan, Italy*
[2]*Department of Civil and Environmental Engineering, Politecnico di Milano, Milan, Italy*

SUMMARY

Replacement beam formulations represent a family of 1D continuum models suitable for approximate analyses of the structural arrangements of buildings. In this paper, an energy equivalence approach is applied to coupled shear walls to develop suitable replacement beam models. Assuming properly compatible coupling fields between walls, a novel three-field coupled two-beam approach, therein providing shear and axial deformations, is proposed. The corresponding mathematical formulation provides closed-form solutions for simple loading cases with homogenous properties. Considering slender coupled shear walls, as typically found in tall buildings, the coupled two beams can be reduced to a two-field formulation, i.e., a parallel assembly of an extensible Euler–Bernoulli beam and a rotation-constraining beam. The latter model is solved analytically, and expressions for the tip displacement and base bending moment are presented. A finite element model is then presented and demonstrated to be an efficient tool for static and dynamic analyses. The effects of the axial deformation and degree of coupling on slender coupled shear wall responses are described as being dependent upon two suitable parameters. Various approximate relations are also proposed for design purposes. Finally, the validity of both analytical solutions and the finite element model is confirmed via numerical examples.

KEY WORDS: coupled shear walls; tall building; continuum approach; coupled two beams (CTB); degree of coupling; axial extensibility

1. INTRODUCTION

Simple continuum formulations, the so-called replacement beams (RBs) (Potzta and Kollar, 2003), can provide useful approximate models for capturing the fundamental response features of a wide class of buildings, especially tall ones (i.e. Tarjian and Kollar, 2004; Zalka, 2001, 2009, 2012; Bozdogan, 2011).

Despite static and dynamic analyses of complex structures can be nowadays easily afforded with the aid of commercial finite element (FE) packages, the adoption of such an approach since an early stage of a design process may be exaggeratedly time consuming and sometimes can lead to an imperfect evolution of the concept (Howson, 2006; Carpinteri *et al*., 2012). Furthermore, computer-based analyses without any checking tools of the outputs may be questionable. The simple continuum-based models can therefore provide a tool for framing the first design phases and to obtain immediate checks of the computer-based analyses; moreover, they help practitioners understand the complex behavior of large structures such as multi-story buildings (Zalka, 2012).

As commonly adopted structural systems, coupled shear walls provide a suitable solution for lateral load resisting systems in tall buildings. The overall stiffness and damping of these structures and their performance are strongly influenced by the properties of the connecting beams. With regard to the composite arrangement of such structures, an equivalent continuum model (e.g. RBs) can be effective in analysis and design processes. To obtain this model, the classical approach in the literature smears

*Correspondence to: Hadi Moghadasi Faridani, Department of Civil and Environmental Engineering, Politecnico di Milano, Milan, Italy
†E-mail: hadi.moghadasi@polimi.it

the stiffness properties of each connecting beam over the inter-story height and considers the solid walls as cantilevers acted upon by lateral loads and laminar shear flows at the junctions with the connecting beams (Coull and Choudhury, 1967; Heidebrecht and Stafford Smith, 1973; Smith and Coull, 1991). Approximate calculations based on the continuum method in which structural elements, such as coupled shear walls, are replaced by a single equivalent sandwich beam have been presented (Tarjian and Kollar, 2004). An approximate method for determining the natural periods of multi-story buildings has been presented (Kaviani *et al*., 2008). In this case, lateral resisting systems are replaced by a cantilever Timoshenko or sandwich beam with varying cross-section.

A proper continuum procedure for the analysis of rows of coupled shear walls can be based on multi-layered beam theory (Capuani *et al*., 1994; 1996), where a displacement-based approach is adopted for the accurate analysis of the static and dynamic responses. Other authors (Savassi and Mancini, 2009) have also developed a one-dimensional FE numerical version based on the continuous medium technique to analyze coupled shear walls and to emphasize the capacity of a correspondingly simple computer code. In addition, a new approximate method has been proposed (Bozdogan *et al*., 2009, Bozdogan, 2009; Bozdogan, 2011) based on the continuum approach, the FE method, and the so-called transfer matrix that is able to simply and efficiently estimate the static and fundamentally dynamic characteristics of coupled walls. Moreover, a method has been proposed (Wdowicki and Wdowicka, 2012) for the analysis of three-dimensional shear walls and shear core assemblies having stepwise changes in the cross-section. This analysis is based on a variant of the continuous connection method and involves replacing the connecting beams by equivalent continuous connections.

Depending on the specific structural arrangement and the effective deformability of the elements, adopting consistent kinematic fields in the RB models may greatly influence their efficiency. It is well established that axial deformations in vertical elements play a fundamental role in the structural response of tall structures (Georgoussis, 2006; 2007). A simple rod theory with a numerical solution (finite difference method) that considers global deformations has been proposed for coupled shear walls (Takabatake, 2010) and for frame tubes (Takabatake *et al*., 1995; Takabatake and Satoh, 2006). The effectiveness was demonstrated through a comparison with FE results for various tall and high-rise buildings. Other authors (Lee *et al*., 2002; Myoungsu *et al*., 2012) have conducted parametric studies on the variation in the axial and bending stiffness properties of columns and beams, therein reporting that the axial stiffness of the columns is the most influential factor in the tube action as well as in the shear lag behavior, whereas the bending stiffness of the columns and beams had little impact, perhaps due to the tube-to-tube interaction. Other studies (Swaddiwudhipong *et al*., 2001; 2002) have stressed that the effect of axial deformation in the frame within frame-shear wall systems should also be considered for tall and/or slender buildings, and the effect of the axial force in the column should be included for arrangements that include a termination of core walls in the lower portion of the building. The axial deformation has been considered in panel-like structures (Mancini and Savassi, 1999, 2004), and a numerical model with cubic one-dimensional FEs was presented to solve the governing equations. The shear deformation was neglected in the formulation. Single-field models with analytical solutions have been proposed to estimate the static solution (Smith and Coull, 1991; Zalka, 2009), and a frequency analysis (Zalka, 2001) of buildings containing coupled walls was developed by introducing axial extensibility into vertical elements. The procedures do not consider the shear and axial deformations as independent fields; rather, they only consider the lateral displacement field in the solution.

Given the importance of compatible kinematical fields such as the shear and axial deformations in walls in addition to the lateral deflection, this paper presents novel continuum models for coupled shear walls without jeopardizing the intrinsic simplicity of the continuum approach. Because of the physical properties of such continuum systems, the models can be applied to FE formulations, especially for dynamic applications, in a straightforward manner compared with previous formulations. Reinoso and Miranda (2005) proposed an equivalent continuum system, which consists of a combination of a flexural beam and a shear beam (SB) in order to simply approximate dynamic characteristics of buildings.

Assuming uniform properties along the height and other consistent assumptions, the coupled shear wall system is reasonably generalized by smearing the properties of spandrel connecting beams into an

equivalent continuum core and using appropriate elastic properties. This continuum model is used as the framework in this study to develop RB systems, although it presents the drawback of its inability to capture the real pure shear mode. Accounting for the independent rotation field and an equal axial field in shear walls induced by global bending effects, a three-field coupled two-beam approach (CTB) is first presented as an RB model for structures with identical walls. When adopting this formulation for non-identical walls, the different axial fields in the two walls must be considered. This model takes the wall shear deformation into account; this is usually neglected in other RB systems. This generalized CTB consists of a condensed extensible Timoshenko beam (TB) and an SB connected by rigid links. The TB is the joint replacement of the two shear walls, and the SB replaces the effect of the connecting beam. The relevant governing differential equations are derived and analytically solved. Addressing tall building structural systems, the CTB model is simplified into a two-field model, i.e., an extensible Euler–Bernoulli beam (EBB) replaces the slender shear walls, and a rotational constraint beam (RCB) corresponds to the continuum core effect.

Two controlling parameters of walls, the *degree of coupling* and the *degree of axial extensibility*, are introduced, and the transverse and axial deformation expressions are derived from differential equations obtained by the minimization of the total potential energy. The tip displacement and overturning moment in tall coupled shear walls are subsequently examined by the latter CTB formulation and are dependent on the interactions of the controlling parameters. A practical criterion that defines a threshold for the adoption of the two-field CTB method is also suggested. In addition to the exact solutions, alternative approximate formulations with acceptable accuracy are proposed to further simplify the prediction of the tip displacement and overturning moment. To apply these formulations, the evaluation of only the preliminary controlling parameters is required.

Finally, a 1D FE model is introduced as a numerical reference solution for the analytical results obtained using the CTB models. All of the theoretical approaches are verified using the FE software SAP2000 (SAP2000, Advanced 14.1.0, Computers and Structures, Berkeley, California, USA) and various methods from the literature. The numerical investigations show that the axial extensibility of shear walls considerably influences their responses, especially at higher degrees of coupling. Considering the axial effects, the displacement, the wall moment, the wall shear and the rotation all increase, whereas certain responses such as the axial force in the walls and the eigenfrequencies decrease. The decrease in the eigenfrequencies and the change in the dynamic responses are more significant for the fundamental mode. The three-field CTB formulation is demonstrated to be applicable not only for slender coupled walls but also for stocky ones and shear-type systems because it also captures the shear deformation in the walls. The proposed CTB models are sufficiently simple and accurate to be used at both the conceptual design stage and the final analysis and can also be useful for checking the results of more advanced numerical calculations, e.g., FE packages.

2. MATERIAL AND METHODS

Depending on the structural characteristics of building structural systems, several RB models may be used (Potzta and Kollar, 2003) to represent the real stiffness of the system as a whole, each characterizing proper kinematical models. Classical RBs include (Figure 1) (a) EBBs, which are suitable for a first approach in modeling tall buildings; (b) SBs, which can capture the behavior of shear-type buildings;

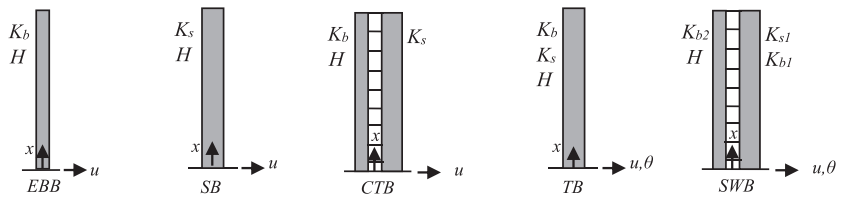

Figure 1. Classical replacement beam models applied as building structural systems. EBB, Euler–Bernoulli beam; SB, shear beam; CTB, coupled two beams; TB, Timoshenko beam; SWB, sandwich beam.

(c) the CTBs, a parallel coupling of an EBB and an SB, which appear appropriate for coupled shear walls and shear wall-frame structures; (d) TBs, a series coupling of an EBB and an SB, which properly model shear walls or trussed resisting schemes; and (e) *sandwich beams*, equivalent to the parallel coupling of the TB and EBB, which is the most general framework and is able to describe the fundamental behavior of frames coupled to single or multiple shear walls.

To develop proper RB models for a coupled shear wall system (Figure 2(a)), a fundamental assumption is required. For this purpose, the discrete set of connecting beams can first be replaced by an equivalent homogeneous core characterized by the elastic moduli E_{eq} and G_{eq}. The resulting system may be assumed as a system (Figure 2(b)) with the following base assumptions:

1. The wall systems are in the plane stress condition.
2. Shear walls have a rigid cross-section, and connecting beams are inextensible.

As suggested in the literature (Capuani *et al*., 1994; 1996), an elastic curtain can be obtained by a stress energy balance between a typical connecting beam and its inter-story equivalent continuum. The equivalent elastic modulus E_{eq} of the continuum core is assumed to be equal to zero to neglect the normal stress component in the core along the vertical axis. The equivalent shear modulus in the continuum core G_{eq} reads (Capuani *et al*., 1994)

$$G_{eq} = \frac{1}{ht}\left(\frac{\ell'^2_b}{12EI_b} + \frac{1}{G\kappa A_b}\right)^{-1} \tag{1}$$

where E and G are the elastic moduli of a typical connecting beam with a moment of inertia I_b and area A_b (the cross-section shear factor) and h and t are the story height and the connecting beam thickness, respectively.

Local deformation effects at junctions between the connecting beams and walls are also taken into account in evaluating the G_{eq} through the following approximate relation

$$\ell'_b \cong \ell_b\left(1 + \mu\frac{h_b}{\ell_b}\right) \tag{2}$$

where h_b and ℓ_b are the connecting beam height and length, respectively. The coefficient μ may be defined in the range $0 < \mu \leq 1$, e.g., $\mu = 0.5$ (Smith and Coull, 1991).

Compatibility between the rotations, $\theta(x)$ and $\psi(x)$, in the shear walls and in the continuum core $\rho(x)$, respectively, at the centroid of the walls can be expressed as (Figure 3(a))

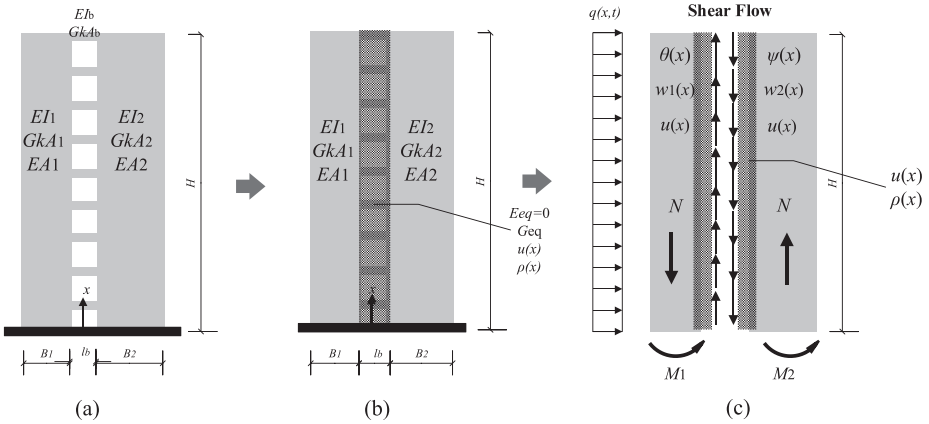

Figure 2. (a) A typical coupled shear wall system, (b) equivalent continuum model, and (c) force equilibrium and consistent kinematical fields.

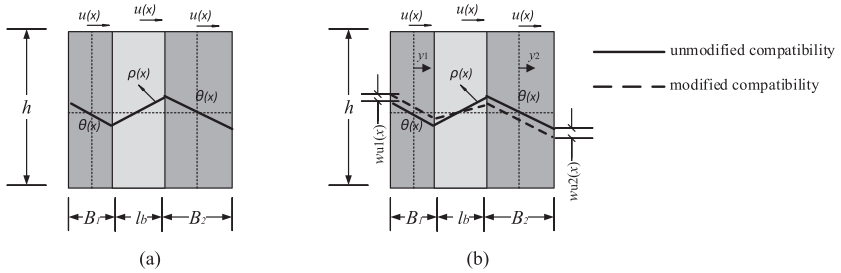

Figure 3. (a) Unmodified and (b) modified rotation compatibilities with axial extensibility in a typical portion of the continuum model.

$$\rho(x) = -\frac{B_1\theta(x) + B_2\psi(x)}{2\ell_b} \tag{3}$$

where B_1 and B_2 are the widths of the left and right shear walls.

Provided that

$$\frac{1}{4} \leq \frac{B_1}{B_2} \leq 4 \tag{4}$$

the rotational fields in the walls are almost identical ($\theta \cong \psi$).

Assuming that the continuum model is subjected to a transverse force, the continuum core plays the role of a transferor between the walls (Figure 2(c)), therein satisfying the equilibrium in the wall internal forces through the shear flow acting vertically inside the core. Thus, an axial extensibility, which is uniformly distributed along the cross-section, is generated in each wall, thereby driving the continuum core to secondarily rotate through its interaction, thus leading to a modification in the compatibility model of the rotation fields (Figure 3(b)). The extensibility fields are shown (Figure 3(b)) as $w_{u1}(x)$ and $w_{u2}(x)$ in the two walls.

However, considering identical rotation in both walls and the modified compatibility, it is convenient to describe the local kinematic fields through the following relations:

$$\begin{cases} w_1(x) = w_{u1}(x) + y_1\theta(x) \\ w_2(x) = -w_{u2}(x) + y_2\theta(x) \end{cases} ;\ \gamma_c(x) = u'(x) - \rho[\theta(x)] - \frac{w_{u1}(x) + w_{u2}(x)}{\ell_b} \tag{5}$$

where $w_1(x)$ and $w_2(x)$ are the total axial displacements in the left and right walls, respectively; y_1 and y_2 are the horizontal distances from the centroids (Figure 3(b)); $\gamma_c(x)$ is the total shear strain in the equivalent continuum core; and $u'(x)$ is the first derivative of the transverse displacement.

The global vertical equilibrium enforces a constraint between the axial strains in the two walls and, thus, between the respective axial extensibilities, i.e., $w_{u1} = -(B_2/B_1)w_{u2}$. For simplicity, in all subsequent analytical formulations, the shear walls are assumed to be identical (i.e. $B_1 = B_2 = B$; $w_{u1} = -w_{u2} = w$). Thus, the normal $\varepsilon_1(x)$, $\varepsilon_2(x)$ and shear $\gamma_1(x)$, $\gamma_2(x)$ strains in the walls read

$$\begin{cases} \varepsilon_1(x) = w_1'(x) = w'(x) + y_1\theta'(x) \ ;\ \gamma_1(x) = u'(x) - \theta(x) \\ \varepsilon_2(x) = w_2'(x) = -w'(x) + y_2\theta'(x) \ ;\ \gamma_2(x) = \gamma_1(x) \end{cases} \tag{6}$$

According to the above assumptions and hypotheses, different continuum-based formulations of coupled shear walls are presented in this paper through the addition or removal of suitable internal kinematic constraints.

2.1. A three-field [u, θ, w] extensible coupled two-beam system

A novel RB model for coupled shear walls, considering the shear deformation and axial extensibility in walls, is introduced on the basis of the continuum model (Figure 2) and the modified compatibility presented in Figure 3(b). This continuum model can be seen (Figure 4) as a single extensible TB and the

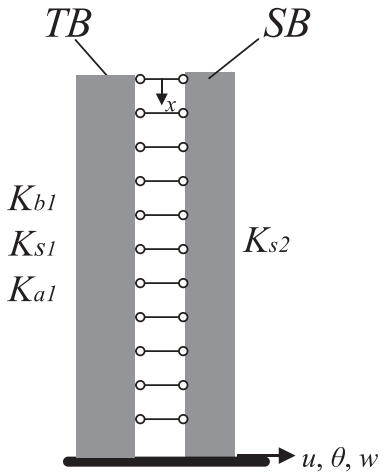

Figure 4. The three-field extensible coupled two-beam model as a parallel coupling of the Timoshenko beam (TB) and sandwich beam (SB) systems.

continuum core as a classical SB, wherein both are connected in parallel by rigid links. This composite system is called the three-field $[u, \theta, w]$ CTB model. It is worth mentioning that the equivalent bending K_{b1}, shear K_{s1} and axial K_{a1} stiffness properties in the TB are obtained by summing the corresponding stiffnesses of the two shear walls, and the equivalent shear stiffness K_{s2} in the SB is proportional to the equivalent shear modulus G_{eq} (refer to Equation (8)). In particular, this CTB system can be prone to model shear-type frames, where the walls and connecting beams, respectively, are converted to inextensible slender columns and stiffened beams. Therefore, the equivalent stiffness properties must be limited properly in the CTB formulation (i.e. $K_{s1} \to \infty; K_{a1} \to \infty; K_{s2} \to \infty$).

Having defined the strains in Equation (6), the total potential energy of a lateral load distribution $q(x)$ consequently reads

$$\begin{aligned} \mathcal{V}(u,\theta,w) = {} & \frac{1}{2}\int_0^H \left[K_{b1}\theta'^2 + K_{a1}w'^2 + K_{s1}(u'-\theta)^2\right] dx + \\ & \frac{1}{2}\int_0^H K_{s2}\left(\frac{B^2}{\ell_b^2}\theta^2 + u'^2 + \frac{4}{{\ell_b}^2}w^2 + \frac{2B}{\ell_b}u'\theta - \frac{4B}{{\ell_b}^2}w\theta - \frac{4}{\ell_b}wu'\right) dx - \int_0^H q(x)u dx \end{aligned} \tag{7}$$

with

$$K_{b1} = 2EI \; ; \; K_{a1} = 2EA \; ; \; K_{s1} = 2G\kappa A \; ; \; K_{s2} = G_{eq}t\ell_b \tag{8}$$

=where A and I are the cross-sectional area and moment of inertia, respectively, of the identical shear walls.

Closed-form solutions of the three-field CTB model acted upon by a transverse load are achieved by solving the differential system arising from the stationarity of Equation (7), i.e.,

$$\begin{cases} u'' - r_0\theta' - r_1 w' - r_2 = 0 \\ \theta'' - r_3\theta + r_4 u' + \left(2BK_{s2}/{\ell_b}^2 K_{b1}\right)w = 0 \\ w'' + \left(2AK_{s2}B/I{\ell_b}^2 K_{b1}\right)\theta + \left(2K_{s2}/\ell_b K_{a1}\right)u' - \left(4K_{s2}/{\ell_b}^2 K_{a1}\right)w = 0 \end{cases} \tag{9}$$

with constants r_0 to r_4 listed in Appendix A. Assuming a constant load q, the system is transformed into a single differential equation as

$$u'''' - r_7 u'' = -r_8\frac{x^2}{2} + r_6 \tag{10}$$

Constants r_6 to r_8 are also presented in Appendix A. The expression of $u(x)$ from Equation (10) is derived as

$$u(x) = C_1 \cosh(\sqrt{r_7}x) + C_2 \sinh(\sqrt{r_7}x) + C_3 + C_4 x - \frac{(r_6 r_7 - r_8)}{2{r_7}^2}x^2 + \frac{r_8}{24 r_7}x^4 \tag{11}$$

By substituting Equation (11) into Equation (9) and solving the set of linear equations, the expressions of the rotational $\theta(x)$ and axial $w(x)$ fields in the shear walls (TB in the CTB model) are given by

$$\theta(x) = \left\{ \frac{r_{11} r_7 \frac{1}{2} - r_1 r_7 \frac{3}{2}}{r_{10}} \left[C_1 \sinh\left(\sqrt{r_7}x\right) + C_2 \cosh\left(\sqrt{r_7}x\right) \right] + \right. \\ \left. \frac{r_{11}}{r_9}\left(C_4 - \frac{r_8}{6 r_7}x^3 \right) + \left(\frac{r_1 r_8 - r_2 r_5 r_{10}}{r_3 r_7} - \frac{r_{11}(r_6 r_7 - r_8)}{r_9 {r_7}^2} \right) x \right\} \tag{12}$$

$$w(x) = \frac{1}{r_1 r_9}\left\{ \left(r_0 r_1 r_7 \frac{3}{2} + r_{12} r_7 \frac{1}{2} \right) [C_1 \sinh(\sqrt{r_7}x) + C_2 \cosh(\sqrt{r_7}x)] + \right. \\ \left. r_{12} C_4 - \frac{r_8 r_{12}}{6 r_7}x^3 + \left(\frac{-r_0 r_1 r_8 + r_0 r_2 r_7 r_{10} - r_2 r_7 r_9}{r_7} - \frac{r_{12}(r_6 r_7 - r_8)}{{r_7}^2} \right) x \right\} \tag{13}$$

with r_9 to r_{12} expressed in Appendix A. The analytical definition of C_1 to C_4 is obtained (Appendix A) by imposing the relevant boundary conditions (origin of x is at the tip point):

$$u(H) = 0 \ ; \ \theta(H) = 0 \ ; \ w(H) = 0 \tag{14}$$

$$\theta'(0) = 0 \ ; \ \ u'(0) - p_1 \theta(0) - p_2 w(0) = 0 \ ; \ w'(0) = 0 \tag{15}$$

The global bending moment $M_G(x)$ is expressed as the sum of the single wall contributions M_L and the overall couple due to axial forces $[N_1(x) = -N_2(x) = N(x)]$:

$$M_G(x) = M_L(x) + N(x)(B + \ell_b) = K_{b1}\theta'(x) + \frac{K_{a1}}{2}(B + \ell_b)w'(x) = \frac{qx^2}{2} \tag{16}$$

The global shear force $V(x)$ can in turn be expressed as follows:

$$V(x) = (K_{s1} + K_{s2})\left[u'(x) + \left(K_{s2}\frac{B}{\ell_b} - K_{s1} \right)\theta(x) - \frac{2K_{s2}}{\ell_b}w(x) \right] = qx \tag{17}$$

where the summation of the first two terms gives the local shear in the walls.

2.2. A two-field [u, w] extensible coupled two-beam model for systems with slender walls

For slender coupled shear walls, the three-field CTB may be further simplified into an axially extensible two-field CTB (Figure 5) composed of an EBB and an RCB. This model is governed by the transverse field $u(x)$ in both the EBB and RCB and by the axial field $w(x)$ only in the EBB, accounting for the extensibility effects in shear walls. In this assembly, the RCB corresponds to the continuum core shown in Figure 2(b). The relevant kinematics of this CTB are obtained by introducing the constraint $\theta = u'$ in both Eqs. (5) and (6).

The relevant definition of the total potential energy reads

$$\mathcal{V}(u, w) = \frac{1}{2}\int_0^H \left[K_{b1} u''^2 + K_{a1} w'^2 \right] dx + \frac{1}{2}\int_0^H K_{s2}\left[\left(1 + \frac{B}{\ell_b} \right)u' - \frac{2}{\ell_b}w \right]^2 dx - \int_0^H q u dx \tag{18}$$

where K_{b1}, K_{a1} and K_{s2} are defined in Equation (8). Note that the second integral in Equation (18) corresponds to the energy contribution of the RCB when the axial effect is considered. Based on such an energy

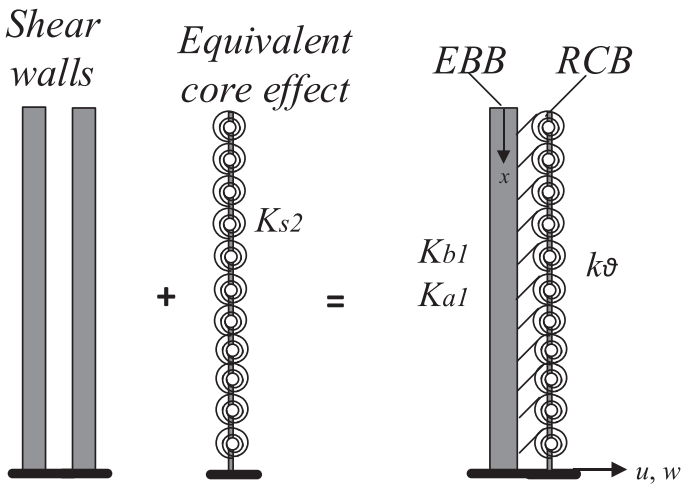

Figure 5. The extensible two-field coupled two-beam model composed of the merged Euler–Bernoulli beam (EBB) constrained by the rational constraint beam (RCB).

definition at the inextensible wall limit (i.e. $w=0$ and $\rho=-(B/\ell_b)u'$), the coupling beam effect reduces to a rotationally distributed stiffness k_ϑ as

$$k_\vartheta = G_{eq}t\ell_b\left(1+\frac{B}{\ell_b}\right)^2 = K_{s2}\left(1+\frac{B}{\ell_b}\right)^2 \tag{19}$$

This coefficient accounts for the level of elastic coupling between the shear walls. For ordinary values of k_ϑ, the response is the combination of the bending and shear behaviors associated with the EBB and RCB, respectively. A value of k_ϑ equal to zero represents a pure flexural model (EBB), and a very large value corresponds to a pure shear-type mode.

Two coupled differential equations in $u(x)$ and $w(x)$ may be achieved by minimizing the energy as follows:

$$\begin{cases} u''''(x)-\alpha\left[u''(x)-\dfrac{2}{d}w'(x)\right]=\dfrac{q(x)}{E\hat{I}} \\ w''(x)-\alpha\dfrac{\hat{I}}{I^*}\left[w(x)-\dfrac{d}{2}u'(x)\right]=0 \end{cases} \tag{20}$$

where

$$\alpha=\frac{k_\vartheta}{E\hat{I}}\ ;\ \hat{I}=2I\ ;\ I^*=\frac{Ad^2}{2}\ ;\ d=(B+\ell_b) \tag{21}$$

The total moment of inertia $\bar{I}$ for the fully coupled wall system (i.e. $k_\vartheta\to\infty$) can then be defined (Smith and Coull, 1991) as

$$\bar{I}=\hat{I}+I^* \tag{22}$$

Two controlling non-dimensional parameters are now introduced in a straightforward manner to clearly evaluate the structural response. The first parameter ξ is called the *degree of axial extensibility* and measures the influence of this source of deformation in the shear wall response. This parameter is the ratio between the axial strain $\varepsilon_A(N)$ of the shear wall and its maximum bending strain $\varepsilon_B(N)$ due to the corresponding transportation moment, $M(N)=N\times d$. This is expressed as

$$\xi = \frac{\varepsilon_A(N)}{\varepsilon_B(N)} = \frac{\frac{Ndx}{EA}}{\frac{M(N)}{2EI}(d/2)dx} = \frac{\hat{I}}{I^*} \tag{23}$$

The second parameter ε is called the *degree of coupling* and controls the degree of participation (e.g. see Reinoso and Miranda, 2005; Kuang and Huang, 2011) of the overall flexural and overall rotational deformations in the CTB system. This defines the elastic constraint between the shear walls in their inextensible configuration:

$$\varepsilon = \alpha H^2 \tag{24}$$

where α is expressed in Equation (21) and H is the total height. Note that the effective amount of coupling, where the wall's extensibility is accounted for, is also controlled by the adjoint parameter ξ.

By considering a distributed constant load q in Equation (20), a single ordinary differential equation in $u(x)$ can be readily derived as

$$u'''' - \frac{\varepsilon(1+\xi)}{H^2}u'' = \frac{q}{E\hat{I}}\left[1 - \frac{\xi\varepsilon}{2}\left(\frac{x}{H}\right)^2\right] \tag{25}$$

The associated boundary conditions are

$$u(H) = 0 \ ; \ u'(H) = 0 \ ; \ w(H) = 0 \tag{26}$$

$$u''(0) = 0 \ ; \ \ u'''(0) - \frac{\varepsilon}{H^2}u'(0) + \frac{2\varepsilon}{dH^2}w(0) = 0 \ ; \ w'(0) = 0 \tag{27}$$

Applying the first equation in Equation (20), those boundary conditions that are dependent on w can be re-expressed in terms of the transverse field $u(x)$ as

$$\frac{dH^2}{2\varepsilon}\left[u'''(H) - \frac{\varepsilon}{H^2}u'(H)\right] = 0 \ \ ; \ \ u''''(0) - \frac{\varepsilon}{H^2}u''(0) = \frac{q}{E\hat{I}} \tag{28}$$

The corresponding expression of $u(x)$ may accordingly be given as follows:

$$\begin{aligned} u(x) = \frac{q}{E\hat{I}\lambda^4 H^2}\Bigg\{ &\left(\frac{x^4 + 12x^2 - 4xH^3 + 3H^4 - 12H^2}{24}\right)\varepsilon\xi + \frac{H^4}{2} + \\ &\frac{H^2}{(1+\xi)}[\,\mathrm{sech}(\lambda H)[-1 + \cosh[\lambda(H-x)] + \lambda H \sinh(\lambda x)] - \lambda H \tanh(\lambda H)]\Bigg\} \end{aligned} \tag{29}$$

where the combined influence of the controlling parameters is expressed by

$$\lambda^2 = (1+\xi)\alpha \tag{30}$$

Substituting Equation (29) into Equation (20), the axial deformation $w(x)$ in the walls is finally expressed as

$$w(x) = \frac{qd}{2}\left\{-\frac{\cosh(\lambda x)}{\lambda^3 E\bar{I}}\left[\tanh(\lambda x) + \frac{\lambda H - \sinh(\lambda H)}{\cosh(\lambda H)}\right] - \frac{2(\xi+1)x}{\lambda^2 E\hat{I}} + \frac{\left(x^3 - H^3\right)}{6E\bar{I}}\right\} \tag{31}$$

The analytical definition of the tip displacement is provided by Equation (29) as

$$u_{tip}^{ex} = \frac{1}{(1+\xi)}\frac{qH^4}{8E\hat{I}}\left\{\frac{4}{(\lambda H)^2} + \xi + \ \frac{8}{(\lambda H)^4\cosh(\lambda H)}[\cosh(\lambda H) - 1 - \lambda H \sinh(\lambda H)]\right\} \tag{32}$$

where λ^2 is defined in Equation (30). The corresponding expression for inextensible shear walls reads

$$u_{tip}^{inex} = \frac{qH^4}{8E\hat{I}}\left\{\frac{4}{(\lambda H)^2} + \frac{8}{(\lambda H)^4\cosh(\lambda H)}[\cosh(\lambda H) - 1 - \lambda H\sinh(\lambda H)]\right\} \tag{33}$$

This latter expression is obtained by assuming $EA \to \infty$ or equivalently by keeping $\xi = 0$ in the definition of λ^2 (Equation (30)). Note that the solution also predicts the expected tip displacement for large degrees of coupling (i.e. $k_\vartheta \to \infty$)

$$\left(u_{tip}^{ex}\right)_{k_\vartheta \to \infty} = \frac{qH^4}{8E\bar{I}} \tag{34}$$

where $\bar{I}$ is defined in Equation (22).

Furthermore, for a very small rotational stiffness k_ϑ, the following asymptotic relation holds:

$$\left(u_{tip}^{ex}\right)_{k_\vartheta \to 0} = \left(u_{tip}^{inex}\right)_{k_\vartheta \to 0} \cong \frac{qH^4}{8E\hat{I}}\left[1 - \frac{\lambda H^2}{3}\right] \tag{35}$$

Uncoupled or fully coupled bending behaviors are attained when $k_\vartheta \to 0$ or $k_\vartheta \to \infty$, respectively. Therefore, various analytical expressions of these conditions are proposed in this section, and their validation is investigated in the model assessment section. The two limiting conditions, called 'uncoupled bending (i.e. *UB*)' and 'fully coupled bending (i.e. *FCB*)', are introduced as

$$UB: \ (k_\theta \to 0 \Rightarrow w \to 0) \ ; \ FCB: \ \left(k_\theta \to \infty \Rightarrow w \to \left(\frac{d}{2}\right)u'\right) \tag{36}$$

By means of the inextensible CTB (i.e. $\xi = 0$), it is also readily verified that for very large values of k_ϑ, the tip displacement vanishes $\left(u_{tip}^{inex}\right)_{k_\vartheta \to \infty} \cong 0$. This can be proven through Equation (33) by applying a very large value of λ. Accordingly, a relevant condition corresponding to inextensible shear walls with a large rotational stiffness k_ϑ may be determined. With regard to the equilibrium, the global bending moment $M_G(x)$ in every two-field CTB model is given by

$$M_G(x) = \left[E\hat{I}u''(x) + \frac{2EI^*}{d}w'(x)\right] = \frac{qx^2}{2} \tag{37}$$

The local bending moment $M_L(x)$ in extensible shear walls can also be derived by considering only the first term in Equation (37). Thus, its expression at the base section is given by

$$M_{bL}^{ex} = \frac{q}{(1+\xi)}\left\{\frac{1}{\lambda^2}[\cosh(\lambda H) + \tanh(\lambda H)[\lambda H - \sinh(\lambda H)] - 1] + \frac{\xi H^2}{2}\right\} \tag{38}$$

For $k_\vartheta \to \infty$, this becomes

$$\left(M_{bL}^{ex}\right)_{k_\vartheta \to \infty} = \frac{qH^2}{2}\frac{\xi}{1+\xi} = \frac{qH^2}{2}\frac{\hat{I}}{\bar{I}} \tag{39}$$

This expression can be compared with its inextensible counterpart

$$M_{bL}^{inex} = \frac{q}{\lambda^2}[\cosh(\lambda H) + \tanh(\lambda H)(\lambda H - \sinh(\lambda H)) - 1] \tag{40}$$

The overturning moment at a very small coupling of the shear walls in both the extensible and inextensible cases is

$$\left(M_{bL}^{ex}\right)_{k_\vartheta \to 0} = \left(M_{bL}^{inex}\right)_{k_\vartheta \to 0} = \frac{qH^2}{2} \tag{41}$$

Furthermore, the shear force in extensible coupled walls can be expressed as follows:

$$V(x) = E\hat{I}\left[u'''(x) - \frac{\lambda^2}{1+\xi}u'(x) + \frac{2\lambda^2}{d(1+\xi)}w(x)\right] = qx \tag{42}$$

2.2.1. On the applicability of the two-field coupled two beams

In this section, a practical limitation is proposed to detect whether the two-field CTB model can be applied instead of the three-field model. For this purpose, the aspect ratio must be introduced for a single shear wall (i.e. $\lambda_1 = B/H$) and a single connecting beam (i.e. $\lambda_2 = l_b/h_b$). The structural responses of 70 coupled shear walls with different aspect ratios are numerically evaluated using the three-field and two-field CTB models, and the difference between their responses is utilized (maximum 5%) as a reliability criterion. It should be noted that the typical inter-story height (i.e. $h = 3$ m) is fixed for all arrangements. Thus, Figure 6 shows the general limitation proposed as a function of the aspect ratios of the walls λ_1 and connecting beams λ_2. For a specific coupled wall system and provided that the point associated with (λ_1 and λ_2) falls into the shaded area, the two-field CTB model can be applied instead of the three-field model with acceptable accuracy; otherwise , the three-field CTB formulation must be used.

2.2.2. Approximate relations for response estimation

Based upon the two controlling parameters of the degree of coupling and the axial extensibility, approximate relations have been introduced that are useful for quick estimation of the tip displacement and the overturning moment. The corresponding expressions are proposed (Table 1) for both uniformly and inversely linear load patterns. An effective inertia ratio function R_1 is recommended in Table 1 for the tip displacement calculations with extensibility effects.

The base local bending moment in the extensible walls can be found using Equation (37) by subtracting the moment produced by the axial forces and the global moment. Accordingly, its expression reads

$$M_{bL} = \frac{qH^2}{j} - dN_b \;\; ; \;\; \begin{cases} j = 2 : Uniform \quad Load \\ j = 3 : Linear \quad Load \end{cases} \tag{43}$$

Consequently, an alternative definition for the axial force at the base N_b can be introduced as

$$N_b = \frac{qH^2}{2d}R_2 \tag{44}$$

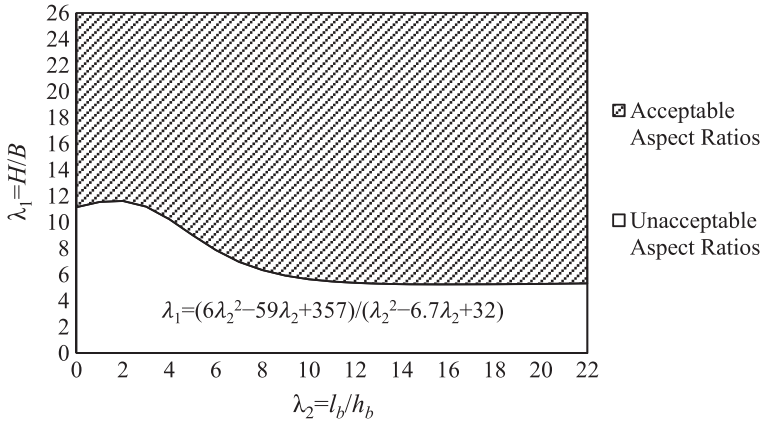

Figure 6. A threshold to confidently use the two-field coupled two-beam model.

Table 1. Alternative formulations of the tip displacement and base bending moment in tall coupled shear walls.

Response	Coupling degree ε	Deflection mode	Uniform load	Linear load
Tip displacement	$\to 0.$	Uncoupled bending	$\frac{qH^4}{8E\bar{I}}.$	$\frac{11qH^4}{120E\bar{I}}.$
	$\to \infty.$	Fully coupled bending	$\frac{qH^4}{8E\bar{I}}.$	$\frac{11qH^4}{120E\bar{I}}.$
	$>0, <\infty.$	Bending shear	$\frac{qH^4}{8E\bar{I}(R_1)}.$	$\frac{11qH^4}{120E\bar{I}(R_1)}$
Base-bending moment	$\to 0$	Uncoupled bending	$\frac{qH^2}{2}$	$\frac{qH^2}{3}$
	$\to \infty$	Fully coupled bending	$\frac{qH^2}{2}\frac{\xi}{\xi+1}$	$\frac{qH^2}{3}\frac{\xi}{\xi+1}$
	$>0, <\infty$	Bending shear	$\frac{qH^2}{2}(1-R_2)$	$\frac{qH^2}{3}(1-R_2)$
	$R_1=\frac{(\varepsilon+2.5)(1+\xi)}{\varepsilon\xi+2.5(1+\xi)}$	$R_2=\frac{5.1(\varepsilon+0.4)}{6(1+\xi)(\varepsilon+5)}$		

where the function R_2 is defined in Table 1. Thus, the overturning moment associated with each load pattern can be directly expressed by substituting Equation (45) into Equation (43). Note that the expression of R_2 is recommended for a practical range of controlling parameters, e.g., $1\leq\varepsilon\leq100$ and $0.1\leq\xi\leq0.33$. The accuracy and simplicity of use of these alternative formulations are demonstrated in the numerical section.

2.3. A three-field [u, θ, w] finite element model

To investigate the static and dynamic responses, the classical FE approach is adopted for the entire equivalent continuum model of Figs. 2(b) and 3(b). A one-dimensional element is therefore introduced for the model with linear variation in the transverse displacement $u(x)$, rotation $\theta(x)$ and axial deformation $w(x)$ in walls, thus resulting in six degrees of freedom (Figure 7). Note that even if the walls are non-identical, a single axial field can be adapted due to the equilibrium of axial forces in the walls. A dimensionless coordinate β and the nodal displacement vector of the e^{th} generic FE are introduced as

$$\beta = 2x/\ell \quad ;; \; U_e = [u_1, \theta_1, w_1, u_2, \theta_2, w_2]^T \tag{45}$$

The generalized displacement vector $\boldsymbol{s}_e(x,t)$ of the e^{th} FE can be expressed as

$$\boldsymbol{s}_e(x,t) = [\, u \quad \theta \quad w \,]^T = \boldsymbol{Z}(x)\boldsymbol{U}_e(t) \tag{46}$$

where $Z(x)$ represents the shape function matrix (see Appendix B).

Upon introducing the relevant Lagrangian $\mathscr{L}$, the transverse equations of motion of the undamped continuum model can be readily obtained by applying Hamilton's principle

$$\delta\int_{t_0}^{t_1}(\mathscr{L})dt = \delta\int_{t_0}^{t_1}\big(T - V + W_q\big)dt = 0 \tag{47}$$

where T is the total kinetic energy, V is the potential energy and W_q is the work produced by the external transverse load. The potential energy is expressed in Equation (7).

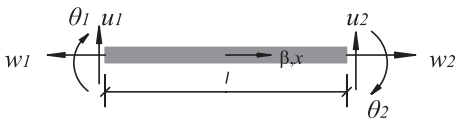

Figure 7. Finite element model for the proposed continuum model with six degrees of freedom.

The kinetic energy reads

$$T(\dot{u}\dot{w}\dot{\theta}) = \frac{1}{2}\int_0^H \left\{ 2\rho_d \left[A(\dot{u})^2 + I(\dot{\theta})^2 + A(\dot{w})^2 \right] + \rho_c \left[A_c(\dot{u}^2) + I_c(\dot{\rho}^2) + \frac{4I_c}{\ell_b{}^2} \right] (\dot{w})^2 \right\} dx \tag{48}$$

where ρ_d is the wall's density; A_c and I_c are the continuum core area and moment of inertia, respectively; and ρ_c represents the core mass per unit volume, with (Capuani *et al*., 1994)

$$\rho_c = \frac{h_b}{h}\rho_d \tag{49}$$

where h_b is the connecting beam height.

Finally, the work due to the external distributed load $q(x,t)$ is given by the subsequent expression

$$W_q = \int_0^H q(x,t)u\, dx \tag{50}$$

To overcome the shear locking effect, a selective reduced integration of the shear-dependent components in the elastic energy is adopted (Capsoni *et al*., 2013). The resulting system of equations of motion of the FE assumes the subsequent expression

$$M_e\ddot{U}_e + C_e\ \dot{U}_e + K_e\ U_e = Q_e \tag{51}$$

M_e and K_e represent the mass and stiffness matrices of the e^{th} generic FE (Appendix B), respectively, and Q_e refers to the generalized force vector. The damping matrix C_e can also be defined based on the classical (proportional) or the non-classical damping and will be the subject of further studies. A free vibration analysis can be performed using Equation (51) by imposing $Q_e = 0$ and performing an eigenanalysis.

3. MODEL ASSESSMENT

All the continuum-based models presented are verified with benchmarks and through cross checks. A 20-story coupled shear wall structure (Figure 8) with an asymmetrical (System 1) or symmetrical (System 2) configuration is assumed as the reference example. Moreover, a multi-story frame (System 3) is presented to examine the capability of the present models in analyzing shear-type structures (Figure 8).

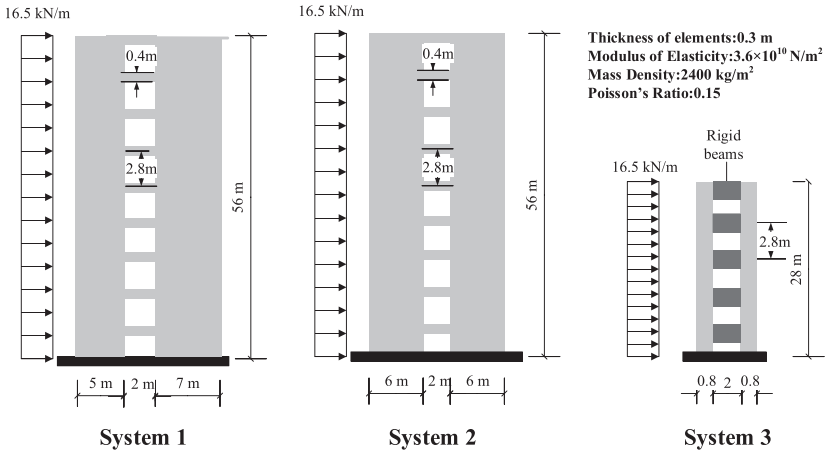

Figure 8. Coupled shear walls (20 stories): System 1 and System 2; Shear frame (10 stories): System 3.

3.1. *Verification of the finite element formulation*

This section refers to System 1 and System 3, which are shown in Figure 8. Because the condition in Equation (4) is satisfied, the FE model with 20 elements can be confidently adopted. To define the stiffness matrix of the FE for System 3, the shear stiffnesses K_{s1} and K_{s2} and the axial stiffness K_{a1} are infinitely magnified. The effectiveness of the proposed continuum-based model is demonstrated with regard to static displacement and free vibration problems by comparison with the results of a FEM software SAP2000 (SAP2000, Advanced 14.1.0, Computers and Structures, Berkeley, California, USA), whereas all the structural members are modeled by shell elements. The first four natural frequencies of System 1 and System 3 are calculated using the proposed FE model and compared (Table 2), respectively, to those found in the literature (Takabatake, 2010; Bozdogan, 2011) and those computed by SAP2000; the results are found to be in agreement with the maximum error of 5.3% for System 3. The static transverse displacement of System 1 is also compared (Figure 9(a)) with those resulting from the various methods, therein showing a stiffer deflection with respect to the solution of Smith and Coull (1991) and SAP2000 model and a smoother one compared with the solution of Takabatake (2010).

3.2. *Verification of three-field and two-field coupled two-beam systems*

The transversal displacement of System 3 resulted by the three-field CTB formulation is compared (Figure 9(b)) with the response obtained from SAP2000 model. Figure 9(b) indicates the good agreement between the two results with a maximum error of 4% at the top, showing that the CTB formulation is approximately capable of modeling shear-type frame systems. It should be noted that the both shear stiffnesses (i.e. K_{s1} and K_{s2}) and the axial stiffness (i.e. K_{a1}) in the CTB formulation are infinitely maximized. Figure 10(a) compares the transverse displacement computed by SAP2000 with the results of the present FE formulation consisting of 20 elements and the three-field CTB solution, all applied to System 2 (Figure 8). The continuum-based graphs are in good agreement with the relatively stiffer response with respect to the result obtained from SAP2000 model. It should be mentioned that these comparisons are conducted based on similar conditions applied in the three-field CTB model.

The accuracy of the analytical solution of the two-field CTB is also investigated based on System 2 using software SAP2000 and analytical expressions presented in the literature (Zalka, 2009; Smith and Coull, 1991). The criterion proposed in Section 2.2.1 is satisfied for the present example to allow using the two-field CTB. The transverse deflection provided by the two-field CTB and the other methods are compared in Figure 10(b). This figure shows that the deflection obtained from SAP2000 model is smoother than the result of the CTB model. Note that the shear deformation in the walls is also considered in SAP2000 model, whereas it is neglected in the CTB. The results by the CTB and Smith and Coull (1991) are perfectly in agreement, although the solution of Zalka (2009) differs, only approaching the other responses at the top. This deflection shape seems to be related to the approximated stiffnesses and the interaction of the shear and flexural behaviors present in Zalka's formulation.

Based on the hypotheses adopted for the three-field CTB system, this model is applicable not only for tall coupled walls but also for short ones, because it can capture the shear deformation in shear walls. To better clarify this point, the difference between the tip displacement by the FE and those obtained using the three-field CTB and literature models (Smith and Coull, 1991; Zalka, 2009) is plotted (Figure 11(a)) as a function of the aspect ratio of a single shear wall ($\lambda_1 = H/B$). It is assumed that the characteristics of the coupling beams are invariant in all the models. According to Figure 11(a), the response difference with respect to the literature models increases dramatically when λ_1 is less than 4

Table 2. First four natural frequencies of System 1 and System 3.

	System 1			System 3	
Mode number	FEM—Takabatake (2010)	Bozdogan (2011)	Present FE	SAP2000	Present FE
1	13.09	13.15	13.08	56.14	53.53
2	55.55	56.66	54.34	188	178
3	129.00	133.03	129.22	358.3	349.18
4	224.90	231.40	229.50	505.1	512.17

FEM, finite element model.

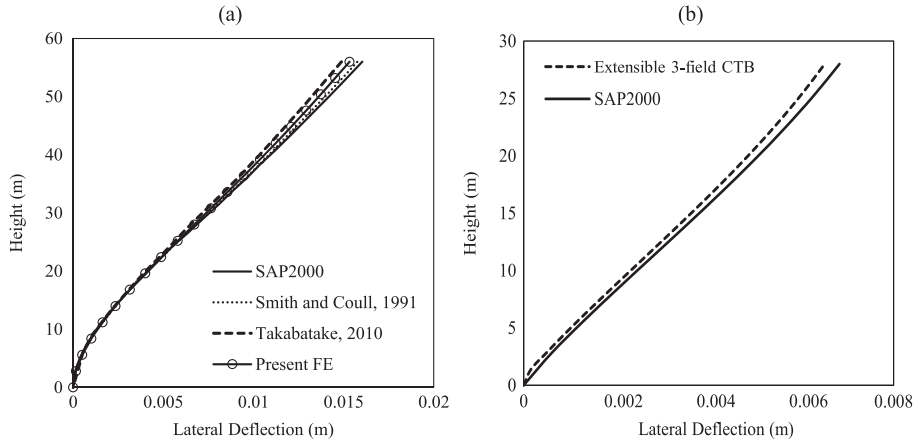

Figure 9. Lateral displacement of (a) System 1 and (b) System 3 due to a uniform load plotted for the present models and other methods. CTB, coupled two beams; FE, finite element.

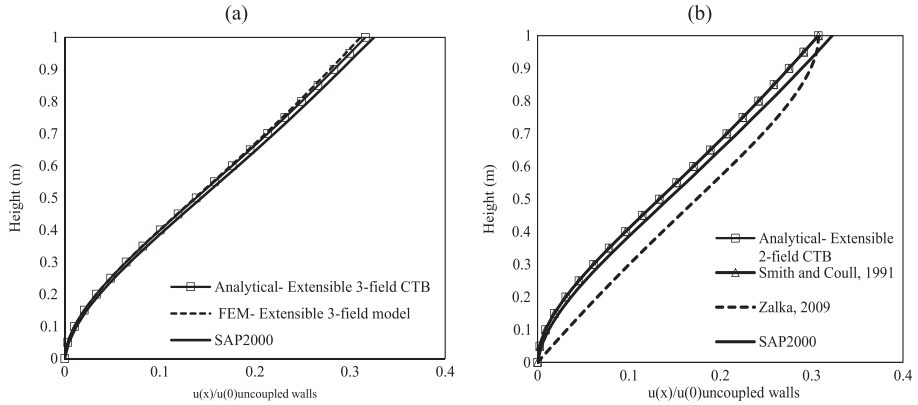

Figure 10. Lateral displacement of System 2 due to a lateral load plotted by (a) SAP2000, present extensible finite element (FE) and three-field coupled two-beam (CTB) model and (b) SAP2000, Zalka's solution, Smith's model and extensible two-field CTB model.

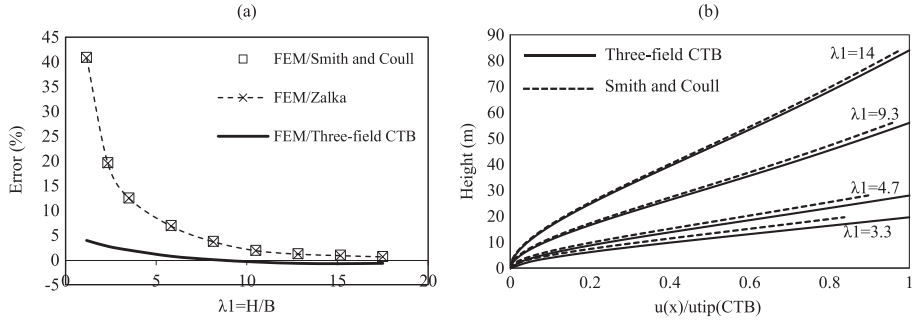

Figure 11. (a) Trend of difference in the tip displacement by analytical formulations with respect to the finite element (FE) response and (b) comparison of the three-field coupled two beams (CTB) and another method for different aspect ratios.

(i.e. the structures are becoming shorter and shorter). This demonstrates that the analytical models proposed in the literature are unable to accurately capture the shear deformation effects in short walls. Increasing the λ_1, the diagrams tend to be more stable, with small errors due to the negligible shear

deformation in the walls. This advantage of the three-field CTB can be observed clearly in Figure 11(b), where its solution is plotted versus that of Smith and Coull (1991) for several aspect ratios.

3.3. Assessment of limiting conditions for the two-field coupled two-beam system

The two limiting conditions presented in Equation (36) are shown for System 2 in Figure 12. The first condition provides almost zero axial deformation ($w \to 0$), as was expected (Figure 12(a)). On the other hand, the 'fully coupled bending' state, attained for large values of k_ϑ, shows that the axial deformation w tends to the slope of the transverse deflection multiplied by $(B+\ell_b)/2$. Diagrams for the axial deflection $w(x)$ and deflection slope $u'(x)$ are graphed in Figure 12(a), showing that the relationship between $w(x)$ and $u'(x)$ is validated when the axial diagram values are approximately four times those of the slope curve $[(B+\ell_b)/2 = (6+2)/2 = 4]$. For instance, with respect to the top elevation response, the axial displacement and the deflection slope are $w = 0.0007844$ *m* and $u' = 0.00019626$ *rad*, respectively, with a ratio of 3.9967. The deflection shapes corresponding to these two state conditions are indicated in Figure 12(b). The corresponding deflection mode for intermediate values of rotational stiffness, i.e., $(0 < k_\vartheta < \infty)$ is bounded by the two plotted curves.

4. NUMERICAL INVESTIGATIONS

Satisfying the criterion proposed in Figure 6, the relevant two-field CTB is applied to analyze System 2. The transversal displacement is plotted in Figure 13(a), with and without the contribution of axial effects. Note that the inextensible wall response can be achieved by assuming $K_{a1} \to \infty$ (i.e. $\xi \to 0$) in all of the formulations. The considerable difference between the two diagrams can be observed, with a maximum of 31% observed at the top. An analogous comparative investigation on the local bending moment, shear force and axial force distribution along the shear walls is conducted (Figures 13(b) and 14(a) and (b)). The maximum differences between the responses of the extensible and inextensible systems are approximately 13%, 20% and 12%, respectively.

The tip displacement is plotted in Figure 15 as function of the degree of coupling ε for different values of the degree of extensibility ξ normalized with respect to the response in the uncoupled bending mode when $\varepsilon = 0$. Note that the tip displacement increases with ξ, with the lowest curve corresponding to the inextensible limit ($\xi = 0$). The range $0 \le \xi \le 1/3$ is considered, where the lower bound applies when the shear walls are a considerable distance from each other, and the upper bound refers to the case of coupling beams with vanishing lengths. A horizontal asymptote, the so-called shear mode state, is specified in Figure 15 for $\xi = 0$ (inextensible walls). In this case, for large ε, the structure is found to exhibit a global shearing mode. It is worth mentioning that because the real shear mode in a frame-type structure contains the subsequent local bending, which occurs among columns and beams, the present CTB formulation cannot exactly capture this mode state due to its uniform continuum. For reference System 2 ($\varepsilon = 10.76$) with extensible ($\xi = 0.1875$) and inextensible ($\xi = 0$) walls, normalized responses of 0.31

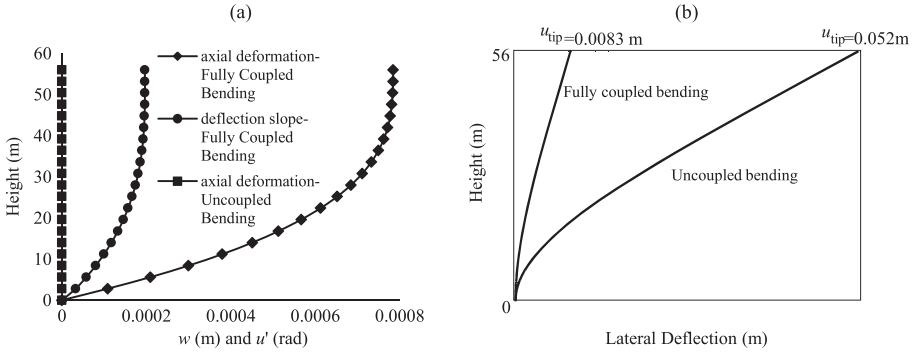

Figure 12. Distribution of (a) axial deformation and slope (b) lateral deflection in the reference coupled shear wall system at two state conditions: uncoupled and fully coupled bending.

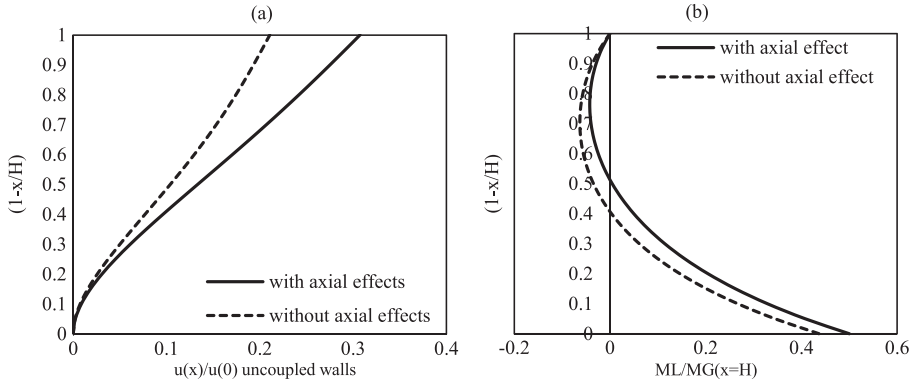

Figure 13. Distribution of (a) the normalized lateral displacement and (b) the normalized bending moment in System 2 due to the uniform load plotted for the two-field coupled two beams for extensible and inextensible shear walls.

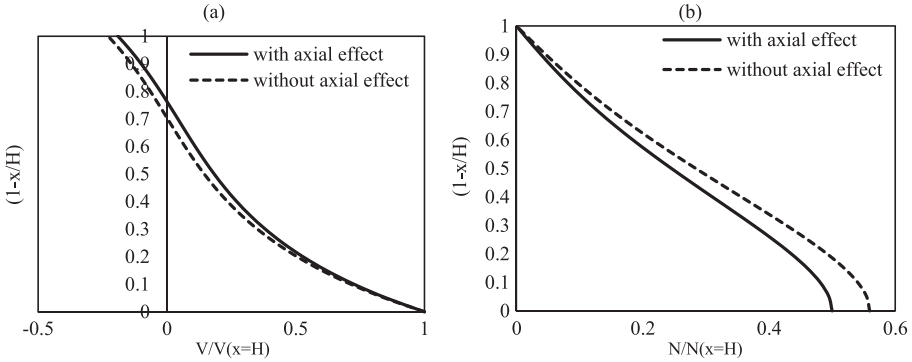

Figure 14. Distribution of (a) the normalized shear force and (b) the normalized axial force in the shear walls of System 2 due to the uniform load plotted for the two-field coupled two beams for extensible and inextensible shear walls.

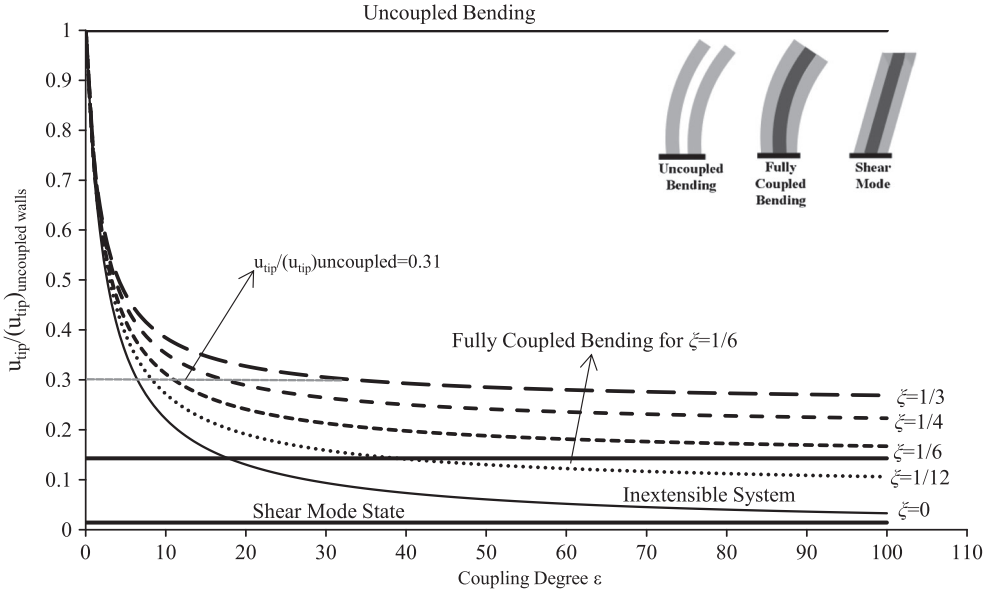

Figure 15. Trend of normalized tip displacement for the coupled shear wall system with different degrees of coupling ε and axial effects ξ in the walls.

and 0.21, respectively, can be attained from Figure (15). For small coupling ($\varepsilon \to 0$), all of the curves tend to approach each other, and the same unit response is found (i.e. uncoupled bending state). A horizontal asymptotic line is specified for this state in Figure (15). The tip displacement for this condition (i.e. 0.05217 m in reference System 2) can be accurately provided using Equation (35). Note that for $\varepsilon \to \infty$, a 'fully coupled bending' state can be assigned to each extensibility level ξ except for $\xi = 0$ (inextensible case). For instance, the typical asymptote for such a state mode is highlighted for $\xi = 1/6$ in Figure (15). The key parameter defining this state is the total inertia $\overline{I} = \overline{I} + I^*$, as defined in Equation (22). The gray dashed line in Figure (15) shows how the same responses can be obtained for different values of ξ and ε. A synoptic frame for the aforementioned behavioral scenarios is presented in Table 3. Using this classification, the tip displacement u_{tip} level in coupled shear walls can be properly evaluated by adopting the relevant expression.

In addition to the tip displacement, the base bending moment is investigated. First, the global base moment M_G is analyzed, considering the extensible ($\xi > 0$) and inextensible ($\xi = 0$) wall formulations. The global base moment, herein normalized with respect to the moment at the uncoupled bending state, is found to be approximately constant for a wide range of values of ε. This is in agreement with the quite obvious equilibrium considerations. The local bending moment M_{bL} at the base of the walls is plotted in Figure (16), normalized with respect to the moment at the uncoupled bending state. Note that all of the curves give the same value for $\varepsilon \to 0$, corresponding to the 'uncoupled bending' state (Equation (41)). It should be noted that the local overturning moment tends to the global one by decreasing ε for both the extensible and inextensible systems. Figure 16 shows that the responses increase with increasing ξ. The corresponding responses in reference System 2 are 0.5 and 0.44 for extensible and inextensible walls, respectively. Upon improving ε, the diagrams tend to exhibit lower base moments, but it is clear that the curve corresponding to the inextensible walls ($\xi = 0$) predicts lower values in comparison with the extensible systems ($\xi > 0$). Similarly to the tip displacement plot, the three limiting conditions are specified by horizontal asymptotic lines and typical deflection shapes in Figure 16. A synoptic frame is also given in Table 4 for the prediction of the local base overturning moment.

To demonstrate the use of the alternative formulations presented in Table 1, the proposed functions R_1 and R_2 are plotted in Figure 17(a) and (b) for practical values of ε and ξ to easily estimate and substitute them into the tip displacement and overturning moment expressions. Moreover, the probable error percentages between the exact and alternative responses are plotted in Figure 17(c) and (d), respectively. These latter plots are obtained by analyzing several structural dimensions of coupled shear walls. Figure 18(c) and (d) shows that the maximum error is approximately 7% in both cases. For System 2, $R_1 = 3.158$ and $R_2 = 0.507$ can be obtained from Table 1 and applied to calculate the tip displacement 0.0165 m and the base moment 12755 kNm, where the errors with respect to the exact responses are 2.48% and 1.42%, Analyzing many arrangements with different structural characteristics, the average difference between the responses of structures with extensible and inextensible walls is plotted (Figure 18) with respect to ε. Note that ξ is fixed in this investigation. Figure 18 indicates that a larger ε produces higher estimation errors, where the axial extensibility is accounted for. It can be observed that the absolute differences in the tip displacement are considerably higher than the errors in the bending moment.

Table 3. General framework for tip displacement in tall building coupled shear walls.

Axial effect parameter	Extensibility status in shear walls	Coupling degree ε	Deflection mode	$u_{tip}(m)$
$\xi = 0$	Inextensible walls	$\to 0$	Uncoupled bending	Eq. (35)
		$\to \infty$	Shear mode state	0.00
		$> 0, < \infty$	Bending shear	Eq. (33)
$0 < \xi \leq 1/3$	Extensible walls	$\to 0$	Uncoupled bending	Eq. (35)
		$\to \infty$	Fully coupled bending	Eq. (34)
		$> 0, < \infty$	Bending shear	Eq. (32)

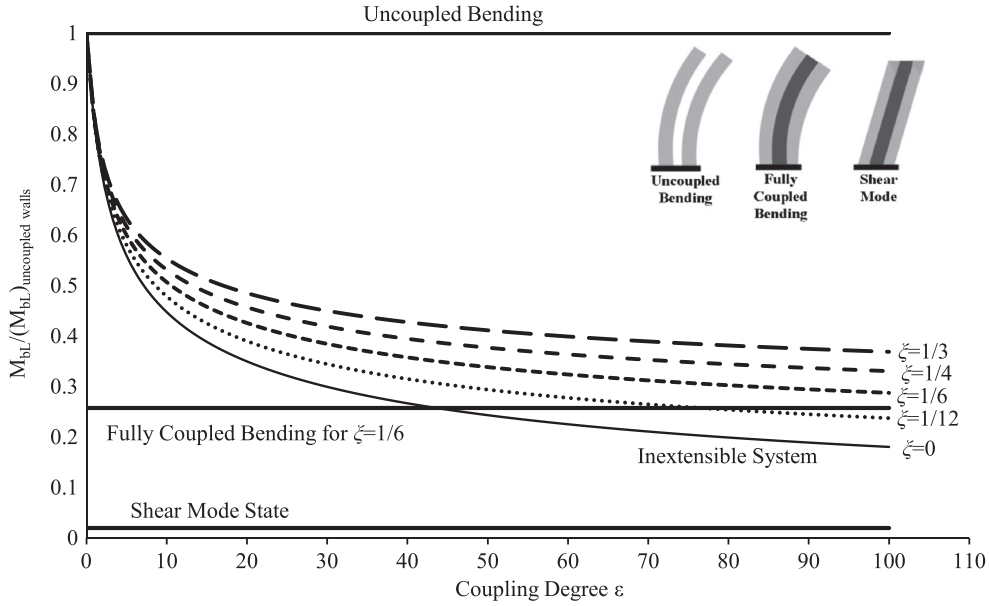

Figure 16. Trend of total base bending moment in only the shear walls in a coupled shear wall system with different degrees of coupling ε and axial effects ξ in the walls.

Table 4. General framework of the local base bending moment in tall building coupled shear walls.

Axial effect parameter	Extensibility status in shear walls	Coupling degree ε	Deflection mode	$\boldsymbol{M_L}$ $(\boldsymbol{N-m})$
$\boldsymbol{\xi=0}$	Inextensible walls	$\rightarrow 0$	Uncoupled bending	Eq. (41)
		$\rightarrow \infty$	Shear mode state	0.00
		$>0, <\infty$	Bending shear	Eq. (40)
$\boldsymbol{0<\xi\leq 1/3}$	Extensible walls	$\rightarrow 0$	Uncoupled bending	Eq. (41)
		$\rightarrow \infty$	Fully coupled bending	Eq. (39)
		$>0, <\infty$	Bending shear	Eq. (38)

The rotation field θ is analyzed here using the three-field CTB model (Equation (12)). This field in reference System 2 is plotted in Figure 19(a), where the extensible case clearly obtains higher values. The maximum rotation locations for the extensible and inextensible walls are placed at considerably different elevations (see small circles on curves in Figure 19(a)). These elevations reveal important information regarding the optimum damping location when addressing damper installation in the dynamic response control.

Therefore, an investigation is conducted with respect to those locations' sensitivity to the degree of coupling in coupled shear walls (Figure 19(b)). The vertical axis in Figure 19(b) refers to the normalized position of the maximum rotation with respect to the total height of the walls. Note that for very low degrees of coupling, both the extensible and inextensible systems give the same values, whereas the two diagrams diverge significantly with increasing coupling degree.

With regard to the frequency-dependent responses, Figure 20(a) and (b) is a plot based on the proposed FE formulation. Figure 20(a) indicates the frequency ratio ω_I/ω_E of systems with inextensible and extensible walls using their first three eigenmodes. To obtain the response of the inextensible case, a very large axial stiffness ($K_{a1}\rightarrow\infty$) is adopted in the FE formulation. The ratio increases with increasing ε, but its magnitude is significantly greater in the fundamental mode and subsequently in the second mode in comparison with the third mode. However, the investigation demonstrates that the extensibility effect in tall coupled shear walls might affect the dynamic responses as well as the static responses. Figure 20(b) compares the dynamic magnification factor of the tip displacement

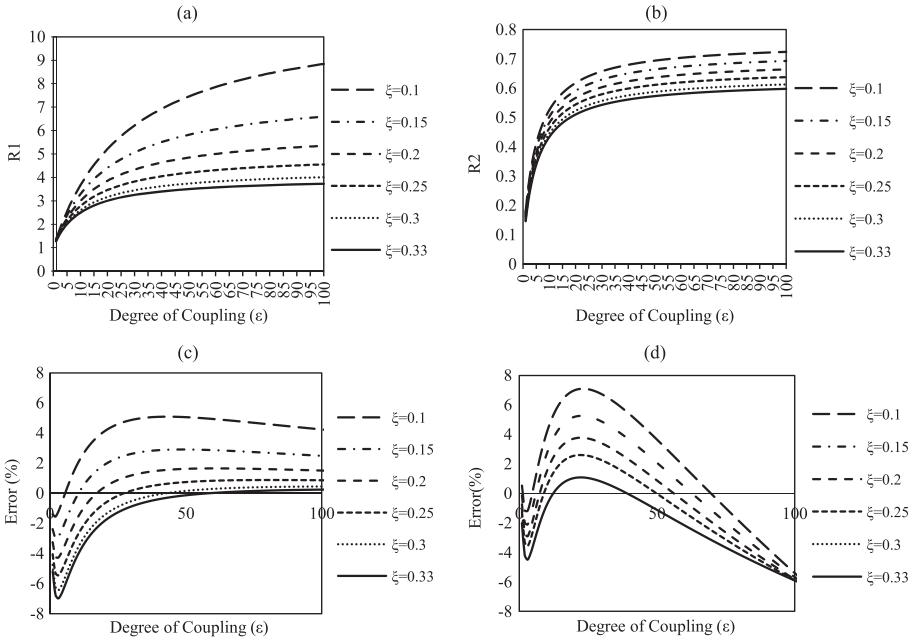

Figure 17. The effective inertia ratio functions (a) R_1 for the tip displacement, (b) R_2 for the overturning moment in coupled shear walls with (c) the error between the exact and approximate tip displacement and (d) the error between the exact and approximate base bending moment.

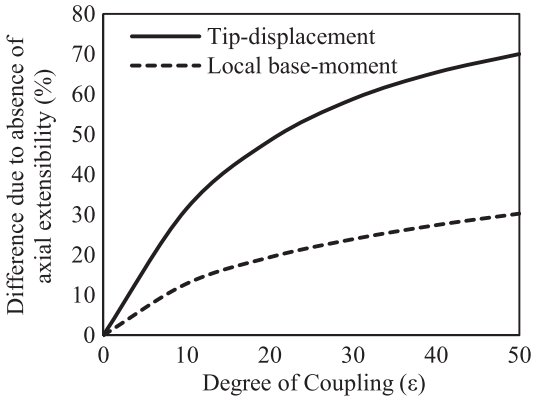

Figure 18. The response difference between extensible and inextensible coupled shear walls versus the degree of coupling.

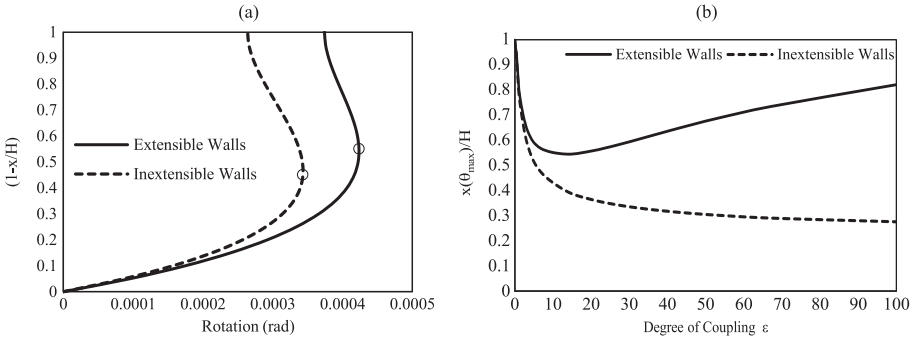

Figure 19. (a) Distribution of the rotation along System 2 with extensible and inextensible coupled walls and (b) distribution of the maximum rotation along the height versus the degree of coupling.

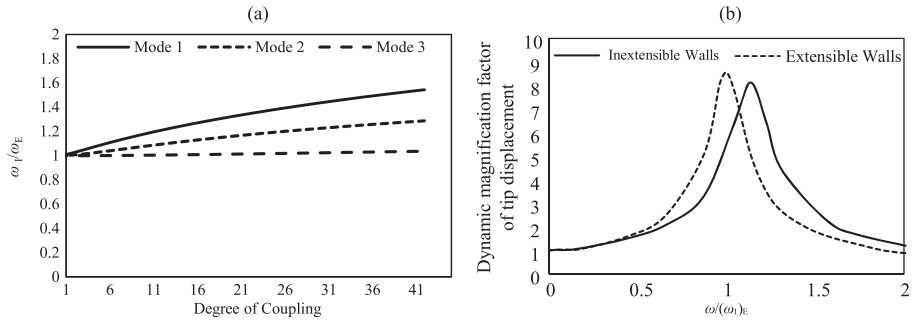

Figure 20. (a) Ratios between modal frequencies in inextensible and extensible coupled walls and (b) dynamic magnification factor of tip displacement versus frequency load ratio in System 2.

between systems with inextensible and extensible walls subject to 5% classical damping. This factor shows the magnification of the static tip displacement when the system is subjected to a harmonic force. Note that the horizontal axis is normalized with respect to the frequency of the extensible structure. Note that the response with axial extensibility differs significantly compared with that without that effect.

5. CONCLUSIONS

A continuum model for coupled shear walls in which the discrete set of connecting beams is replaced by an equivalent elastic core has been developed. Based on this framework, two novel CTB models considering the axial deformation in the walls and a one-dimensional FE model used to facilitate the dynamic analysis of coupled walls are developed. The range of application of the two CTB formulations depends on the shear walls' slenderness. These formulations refer to systems with identical shear walls, but generalization is straightforward provided that the ratio between the dimensions of the walls is limited. The closed-form formulation of the models is properly derived and further developed for the novel CTB with solutions depending on two controlling parameters: the *degree of coupling* and the *degree of axial extensibility*. The analysis of a reference structure shows that the transverse deflection, local bending moment, wall axial force, wall shear and wall rotation distributions when considering extensibility in the walls can differ considerably from the corresponding inextensible counterparts. This difference increases for increasing degrees of coupling and is particularly important in the displacement components. The analysis of the limiting conditions of 'uncoupled bending', 'fully coupled bending' and pure 'shear mode state', depending on values assumed by the two controlling parameters, highlights the role of extensibility, especially for slender coupled shear walls. With respect to the dynamic response, axial extensibility reduces the natural eigenfrequencies, especially the first one, and may significantly change the forced response. The investigations showed that the extensible two-field CTB cannot capture the pure 'shear mode state' featuring stocky walls; however, it reveals a suitable RB model for a wide range of practical wall slendernesses. Also, the capability of the CTB formulation was verified in modeling shear-type frames. Various easy-to-use approximate formulas proposed, based upon the controlling parameters, for the tip displacement and base overturning moment demonstrated their suitability for design purposes. The proposed CTB models may be useful for both researchers and practicing engineers.

APPENDIX A

Symbolic definitions and constants adapted in the solution of the extensible three-field CTB are listed as follows:

$$r_0 = \frac{K_{s1} - K_{s2}(B/\ell_b)}{K_{s1} + K_{s2}}\,;\; r_1 = \frac{2K_{s2}}{\ell_b(K_{s1} + K_{s2})}\,;\; r_2 = \frac{q}{K_{s1} + K_{s2}}\,;\; r_3 = \frac{K_{s1} + K_{s2}(B/\ell_b)^2}{K_{b1}}\,;$$

$$r_4 = \frac{K_{s1} - K_{s2}(B/\ell_b)}{K_{b1}}\,;\; r_5 = \frac{2K_{s2}}{\ell_b K_{a1}} r_6 = \frac{\left(B^2 K_{a1} + 4K_{b1}\right){K_{s2}}^2 - 2BK_{a1}K_{s1}K_{s2}\ell_b + K_{a1}{K_{s1}}^2{\ell_b}^2}{K_{a1}K_{b1}(K_{s1} + K_{s2})^2{\ell_b}^2} q\,;$$

$$r_7 = \frac{K_{s1}K_{s2}\left[4K_{b1} + K_{a1}(B + \ell_b)^2\right]}{K_{a1}K_{b1}(K_{s1} + K_{s2}){\ell_b}^2}$$

$$r_8 = \frac{(2B - \ell_b)(BK_{s2} - K_{s1}\ell_b)\left(-B^2K_{a1}K_{s2} - 4K_{b1}K_{s2} + BK_{a1}K_{s1}\ell_b\right)}{K_{a1}{K_{b1}}^2(K_{s1} + K_{s2}){\ell_b}^4} q$$

$$r_9 = \frac{8ABK_{a1}{K_{s2}}^2 + 2I(BK_{s2} - K_{s1}\ell_b)[-4K_{b1}K_{s2} + K_{a1}K_{s1}\ell_b(B + \ell_b)]}{K_{a1}K_{b1}(K_{s1} + K_{s2})^2{\ell_b}^4 I} K_{s2}$$

$$r_{10} = \frac{2K_{s2}\left(B^2K_{a1}K_{s2} + 4K_{b1}K_{s2} - BK_{a1}K_{s1}\ell_b\right)}{K_{a1}K_{b1}(K_{s1} + K_{s2}){\ell_b}^3}\,;$$

$$r_{11} = \frac{2K_{s1}K_{s2}\left(B^2K_{a1}K_{s2} + 4K_{b1}K_{s2} + BK_{a1}(-K_{s1} + K_{s2})\ell_b - K_{a1}K_{s1}{\ell_b}^2\right)}{K_{a1}K_{b1}(K_{s1} + K_{s2})^2{\ell_b}^3}$$

$$r_{12} = \frac{8ABK_{a1}K_{s2}(K_{s1} + K_{s2}) + 2I(BK_{s2} - K_{s1}\ell_b)\left[-4K_{b1}K_{s2} + K_{a1}K_{s1}(B + \ell_b)^2\right]}{K_{a1}K_{b1}(K_{s1} + K_{s2})^3{\ell_b}^4 I} {K_{s2}}^2$$

$$C_1 = \frac{-r_2r_7(r_0r_4 + r_1r_5) + r_8}{{r_7}^3}\,;\; C_2 = -[\tanh(\sqrt{r_7}H) - \sqrt{r_7}H\,\mathrm{sech}(\sqrt{r_7}H)]C_1$$

$$C_3 = r_2H^2 + \frac{5r_8H^4}{24r_7} + \left[0.5H^2r_7 - \cosh(\sqrt{r_7}H)\right]C_1 - \sinh(\sqrt{r_7}H)C_2\,;\; C_4 = \frac{6r_2r_7H + r_8H^3}{6r_7}$$

APPENDIX B

The matrix, including the shape functions selected for the FE, reads as follows:

$$\boldsymbol{Z}(x) = \begin{bmatrix} Z_1 & 0 & 0 & Z_2 & 0 & 0 \\ 0 & Z_1 & 0 & 0 & Z_2 & 0 \\ 0 & 0 & Z_1 & 0 & 0 & Z_2 \end{bmatrix} = \frac{1}{2}\begin{bmatrix} 1-\beta & 0 & 0 & 1+\beta & 0 & 0 \\ 0 & 1-\beta & 0 & 0 & 1+\beta & 0 \\ 0 & 0 & 1-\beta & 0 & 0 & 1+\beta \end{bmatrix}$$

The stiffness matrix of the FE with length ℓ associated with extensible walls and continuum core are, respectively,

$$K_{walls} = \ell\begin{bmatrix} K_{s1}/\ell^2 & K_{s1}/\ell/2 & 0 & -K_{s1}/\ell^2 & K_{s1}/\ell/2 & 0 \\ K_{s1}/\ell/2 & K_{b1}/\ell^2 + K_{s1}/4 & 0 & -K_{s1}/\ell/2 & -K_{b1}/\ell^2 + K_{s1}/4 & 0 \\ 0 & 0 & K_{a1}/\ell^2 & 0 & 0 & -K_{a1}/\ell^2 \\ -K_{s1}/\ell^2 & -K_{s1}/\ell/2 & 0 & K_{s1}/\ell^2 & -K_{s1}/\ell/2 & 0 \\ K_{s1}/\ell/2 & -K_{b1}/\ell^2 + K_{s1}/4 & 0 & -K_{s1}/\ell/2 & K_{b1}/\ell^2 + K_{s1}/4 & 0 \\ 0 & 0 & -K_{a1}/\ell^2 & 0 & 0 & K_{a1}/\ell^2 \end{bmatrix}$$

$$K_{core} = K_{s2}\ell \begin{bmatrix} 1/\ell^2 & -\overline{B}/4/\ell & \overline{D}/4/\ell & -1/\ell^2 & -\overline{B}/4/\ell & \overline{D}/4/\ell \\ -\overline{B}/4/\ell & \overline{A}/4 & -\overline{C}/8 & \overline{B}/4/\ell & \overline{A}/4 & -\overline{C}/8 \\ \overline{D}/4/\ell & -\overline{C}/8 & \overline{F}/4 & -\overline{D}/4/\ell & -\overline{C}/8 & \overline{F}/4 \\ -1/\ell^2 & B/4/\ell & -\overline{D}/4/\ell & 1/\ell^2 & \overline{B}/4/\ell & -\overline{D}/4/\ell \\ -\overline{B}/4/\ell & \overline{A}/4 & -\overline{C}/8 & \overline{B}/4/\ell & \overline{A}/4 & -\overline{C}/8 \\ \overline{D}/4/\ell & -\overline{C}/8 & \overline{F}/4 & -\overline{D}/4/\ell & -\overline{C}/8 & \overline{F}/4 \end{bmatrix}$$

where $\overline{A} = \left[\frac{(B_1+B_2)}{2\ell_b}\right]^2; \overline{B} = \frac{(B_1+B_2)}{\ell_b}\ ;\ \overline{C} = \frac{(B_1+B_2)^2}{\ell_b{}^2 B_1}\ ; \overline{D} = \frac{2}{\ell_b}\frac{(B_1+B_2)}{B_1}\ ; \overline{F} = \frac{1}{\ell_b{}^2}\left[\frac{(B_1+B_2)}{B_1}\right]^2$

Thus, assembling two stiffness matrices yields the global matrix as $K_{\mathrm{e}} = K_{\mathrm{walls}} + K_{\mathrm{core}}$.

The FE mass matrix contribution M_{walls} to the walls and to the equivalent continuum core M_{core} read

$$\mathrm{M}_{\mathrm{walls}} = \frac{\ell}{6}\begin{bmatrix} 2(\gamma_u+\overline{m}) & 0 & 0 & (\gamma_u+\overline{m}) & 0 & 0 \\ 0 & 2\gamma_\theta & 0 & 0 & \gamma_\theta & 0 \\ 0 & 0 & 2\gamma_w & 0 & 0 & \gamma_w \\ (\gamma_u+\overline{m}) & 0 & 0 & 2(\gamma_u+\overline{m}) & 0 & 0 \\ 0 & \gamma_\theta & 0 & 0 & 2\gamma_\theta & 0 \\ 0 & 0 & \gamma_w & 0 & 0 & 2\gamma_w \end{bmatrix}$$

$$\mathrm{M}_{\mathrm{core}} = \frac{\ell}{6}\begin{bmatrix} 2\gamma_{uc} & 0 & 0 & \gamma_{uc} & 0 & 0 \\ 0 & 2\gamma_{\theta c} & 0 & 0 & \gamma_{\theta c} & 0 \\ 0 & 0 & 2\gamma_{wc} & 0 & 0 & \gamma_{wc} \\ \gamma_{uc} & 0 & 0 & 2\gamma_{uc} & 0 & 0 \\ 0 & \gamma_{\theta c} & 0 & 0 & 2\gamma_{\theta c} & 0 \\ 0 & 0 & \gamma_{wc} & 0 & 0 & 2\gamma_{wc} \end{bmatrix}$$

where

$$\gamma_u = \rho_d t(B_1+B_2)\ ;\ \gamma_\theta = \rho_d(I_1+I_2)\ ;\ \gamma_w = \rho_d t\frac{\left(B_1B_2+B_2{}^2\right)}{B_1}; \gamma_{uc} = \rho_d\frac{h_b}{h}t\ell_b\ ;$$

$$\gamma_{\theta c} = \rho_d\frac{h_b t\ell_b{}^3}{h\ 12}\left(\frac{B_1+B_2}{2\ell_b}\right)^2 \gamma_{wc} = \rho_d\frac{h_b t\ell_b{}^3}{h\ 12}\left(\frac{B_1+B_2}{\ell_b B_1}\right)^2$$

Finally, the global mass matrix is $M_{\mathrm{e}} = M_{\mathrm{walls}} + M_{\mathrm{core}}$.

REFERENCES

Bozdogan KB, Ozturk D, Nuhoglu A. 2009. An approximate method for static and dynamic analyses of multi-bay coupled shear walls. *Struct. Design Tall Spec. Build.* **18**(1): 1–12.

Bozdogan KB. 2009. An approximate method for static and dynamic analyses of symmetric wall-frame buildings. *Struct. Design Tall Spec. Build.* **18**(3): 279–290.

Bozdogan KB. 2011. A method for lateral static and dynamic analyses of wall-frame buildings using one dimensional finite element. *Scientific Research and Essays* **6**(3): 616–626.

Capsoni A, Vigano GM, Bani-Hani KH. 2013. On damping effects in Timoshenko beams. *International Journal of Mechanical Sciences* **73**: 27–39.

Capuani D, Merli M, Savoia M. 1994. An equivalent continuum approach for coupled shear walls. *Engineering Structures* **16**(1): 63–73.

Capuani D, Merli M, Savoia M. 1996. Dynamic analysis of coupled shear wall-frame systems. *Journal of Sound and Vibration* **192**(4): 867–883.

Carpinteri A, Corrado M, Lacidogna G, Cammarano S. 2012. Lateral load effects on tall shear wall structures of different height. *Struct. Eng. and Mech.* **41**(3): 313–337.

Coull A, Choudhury JR. 1967. Analysis of coupled shear walls. *Journal ACZ* **64**: 587–593.
Georgoussis GK. 2006. A simple model for assessing periods of vibration and modal response quantities in symmetrical buildings. *Struct. Design Tall Spec. Build* **15**(2): 139–151.
Georgoussis GK. 2007. Approximate analysis of symmetrical structures consisting of different types of bents. *Struct. Design Tall Spec. Build.* **16**(3): 231–247.
Heidebrecht AC, Stafford Smith B. 1973. Approximate analysis of tall wall-frame structures. *Journal of the Structural Division, ASCE* **99**(2): 199–221.
Howson P. 2006. Global analysis: back to the future. *The Structural Engineer* **84**(3): 18–21.
Kaviani P, Rahgozar R, Saffari H. 2008. Approximate analysis of tall buildings using sandwich beam models with variable cross-section. *Struct. Design Tall Spec. Build.* **17**(2): 401–418.
Kuang JS, Huang K. 2011. Simplified multi-degree-of-freedom model for estimation of seismic response of regular wall-frame structures. *Struct. Design Tall Spec. Build.* **20**: 418–432.
Lee KK, Lee LH, Lee EJ. 2002. Prediction of shear-lag effects in framed-tube structures with internal tube(s). *Struct. Design Tall Spec. Build.* **11**: 73–92.
Mancini E, Savassi W. 1999. Tall building structures unified plane panels behavior. *Struct. Design Tall Spec. Build.* **8**(2): 155–170.
Myoungsu S, Thomas HK, Pimentel B. 2012. Towards optimal design of high-rise building tube systems. *truct. Design Tall Spec. Build.* **21**: 447–464.
Reinoso E, Miranda E. 2005. Estimation of floor acceleration demands in high-rise buildings during earthquakes. *Struct Design Tall Spec.* **14**(2): 107–130.
Potzta G, Kollar LP. 2003. Analysis of building structures by replacement sandwich beams. *International Journal of Solids and Structures* **40**(3): 535–553.
SAP2000. nd. Advanced 14.1.0, Computers and Structures, Berkeley, California, USA.
Savassi W, Mancini E. 2004. One-dimensional finite element solution for tall building structures unified plane panels formulation. *Struct. Design Tall Spec. Build.* **13**(4): 315–333.
Savassi W, Mancini E. 2009. One-dimensional finite element solution for non-uniform tall building structures and loading. *Struct. Design Tall Spec. Build.* **18**(4): 441–453.
Smith BS, Coull A. 1991. *Tall Building Structures: Analysis and Design*. John Wily & Sons: New York.
Swaddiwudhipong S, Lee SL, Zhou Q. 2001. Effect of axial deformation on vibration of tall buildings. *Struct. Design Tall Spec.* **10**(2): 79–91.
Swaddiwudhipong S, Sidji S, Lee SL. 2002. The effects of axial deformation and axial force on vibration characteristics of tall buildings. *Struct. Design Tall Spec.* **11**(5): 309–328.
Takabatake H, Takesako R, Kobayashi M. 1995. A simplified analysis of doubly symmetric tube structures. *Struct. Des. Tall Spec. Build.* **4**(2): 137–153.
Takabatake H, Satoh T. 2006. A simplified analysis and vibration control to super-high-rise buildings. *Struct. Design Tall Spec. Build.* **15**(4): 363–390.
Takabatake H. 2010. Two-dimensional rod theory for approximate analysis of building structures. *Earthquakes Struct.* **1**(1): 1–19.
Tarjian G, Kollar LP. 2004. Approximate analysis of building structures with identical stories subjected to earthquake. *International Journal of Solids and Structures* **41**(5): 1411–1433.
Wdowicki J, Wdowicka E. 2012. Analysis of shear wall structures of variable cross section. *Struct. Design Tall Spec. Build.* **21**(1): 1–15.
Zalka AK. 2001. A simplified method for calculation of the natural frequencies of wall-frame buildings. *Engineering Structures* **23**(12): 1544–1555.
Zalka AK. 2009. A simple method for the deflection analysis of tall wall-frame building structures under horizontal load. *Struct. Design Tall Spec. Build.* **18**(3): 291–311.
Zalka AK. 2012. *Structural Analysis of Regular Multi-story Buildings*. CRC Press: Taylor & Francis Group.

AUTHORS' BIOGRAPHIES

Antonio Capsoni is currently an associate Professor of Theory of Structures in Department of Architecture, Built Environment and Construction Engineering at Politecnico di Milano in Italy. His research interests include assessment and retrofit of new and existing bridges and tall buildings, structural dynamics, passive damping, and structural stability.

Hadi Moghadasi Faridani is a PhD candidate in structural engineering in Department of Civil and Environmental Engineering at Politecnico di Milano in Italy. His research interests include finite element method, bridge engineering, static and dynamic assessment of structural systems of tall buildings, and passive damping.